

# Study of $e^+e^- \rightarrow \omega\pi^0 \rightarrow \pi^0\pi^0\gamma$ in the energy range 1.05–2.00 GeV with SND

M. N. Achasov,<sup>1,2</sup> V. M. Aulchenko,<sup>1</sup> A. Yu. Barnyakov,<sup>1</sup> K. I. Beloborodov,<sup>1,2</sup> A. V. Berdyugin,<sup>1,2</sup>  
 A. G. Bogdanchikov,<sup>1</sup> A. A. Botov,<sup>1</sup> T. V. Dimova,<sup>1</sup> V. P. Druzhinin,<sup>1,2</sup> V. B. Golubev,<sup>1,2</sup>  
 K. A. Grevtsov,<sup>1,2</sup> L. V. Kardapoltsev,<sup>1,2,\*</sup> A. G. Kharlamov,<sup>1,2</sup> D. P. Kovrizhin,<sup>1</sup> I. A. Koop,<sup>1,2</sup>  
 A. A. Korol,<sup>1,2</sup> S. V. Koshuba,<sup>1</sup> A. P. Lysenko,<sup>1</sup> K. A. Martin,<sup>1,3</sup> I. N. Nesterenko,<sup>1</sup> A. E. Obrazovsky,<sup>1</sup>  
 E. V. Pakhtusova,<sup>1</sup> E. A. Perevedentsev,<sup>1,2</sup> A. L. Romanov,<sup>1,2</sup> S. I. Serednyakov,<sup>1,2</sup> Z. K. Silagadze,<sup>1,2</sup>  
 K. Yu. Skovpen,<sup>1</sup> A. N. Skrinsky,<sup>1</sup> I. K. Surin,<sup>1</sup> Yu. A. Tikhonov,<sup>1,2</sup> A. V. Vasiljev,<sup>1</sup>  
 P. Yu. Shatunov,<sup>1</sup> Yu. M. Shatunov,<sup>1</sup> D. A. Shtol,<sup>1</sup> A. L. Romanov,<sup>1,2</sup> and I. M. Zemlyansky<sup>1</sup>

<sup>1</sup>*Budker Institute of Nuclear Physics, SB RAS, Novosibirsk, 630090, Russia*

<sup>2</sup>*Novosibirsk State University, Novosibirsk, 630090, Russia*

<sup>3</sup>*Novosibirsk State Technical University, Novosibirsk, 630092, Russia*

The cross section for the process  $e^+e^- \rightarrow \omega\pi^0 \rightarrow \pi^0\pi^0\gamma$  has been measured in the center-of-mass energy range 1.05–2.00 GeV. The experiment has been performed at the  $e^+e^-$  collider VEPP-2000 with the SND detector. The measured  $e^+e^- \rightarrow \omega\pi^0$  cross section above 1.4 GeV is the most accurate to date. Below 1.4 GeV our data are in good agreement with the previous SND and CMD-2 measurements. Data on the  $e^+e^- \rightarrow \omega\pi^0$  cross section are well described by the Vector Meson Dominance (VMD) model with two excited  $\rho$ -like states. From the measured cross section we have extracted the  $\gamma^* \rightarrow \omega\pi^0$  transition form factor. It has been found that the VMD model cannot describe simultaneously our data and data obtained from the  $\omega \rightarrow \pi^0\mu^+\mu^-$  decay. We have also tested Conserved Vector Current (CVC) hypothesis comparing our results on the  $e^+e^- \rightarrow \omega\pi^0$  cross section with data on the  $\tau^- \rightarrow \omega\pi^-\nu_\tau$  decay and have found that the CVC hypothesis works well within reached experimental accuracy of about 5%.

PACS numbers: 13.66.Bc, 14.40.Be, 13.40.Gp, 13.25.Gv

## I. INTRODUCTION

Experiments with the SND detector [2] at the  $e^+e^-$  collider VEPP-2000 [1] started in 2010. The main goals of these experiments are a high precision measurement of the total cross section of  $e^+e^- \rightarrow \text{hadrons}$  in the center-of-mass (c.m.) energy range up to 2 GeV and investigation of the vector meson excitations with masses between 1 and 2 GeV/ $c^2$ . In this connection, a study of the process

$$e^+e^- \rightarrow \omega\pi^0 \rightarrow \pi^0\pi^0\gamma \quad (1)$$

is very topical. The process  $e^+e^- \rightarrow \omega\pi^0$  is one of the dominant hadronic processes contributing to the total hadronic cross section at the c.m. energy between 1 and 2 GeV. As one of the important decay modes of the isovector vector states  $\rho(1450)$  and  $\rho(1700)$ , it can provide a lot of information about their properties. Moreover, this measurement can be used to check the relation between the the  $e^+e^- \rightarrow \omega\pi^0$  cross section and the differential rate in the  $\tau^- \rightarrow \omega\pi^-\nu_\tau$  decay following from the conservation of vector current and isospin symmetry (CVC hypothesis) [3]. The SND plans to search for electric dipole decays of the  $\rho(1450)$  and  $\rho(1700)$  mesons to the  $\pi^0\pi^0\gamma$  final state, which are important for understanding of the  $\rho(1450)$  and  $\rho(1700)$  quark structure. The process  $e^+e^- \rightarrow \omega\pi^0$  is the main background for this search; its precise measurement is the first step in investigating the  $\rho(1450)$  and  $\rho(1700)$  radiative decays.

In this work the process  $e^+e^- \rightarrow \omega\pi^0$  is studied in the  $\omega$  decay mode to  $\pi^0\gamma$ . Despite the fact that the main  $\omega$  decay mode to  $\pi^+\pi^-\pi^0$  has a probability about an order of magnitude higher, this choice looks reasonable. Unlike the  $4\pi$  final state, the  $\omega\pi^0$  intermediate mechanism is dominant in the  $\pi^0\pi^0\gamma$  final state in the energy range under study. This makes it possible to avoid systematic uncertainties due to both the complex procedure of subtracting background and taking into account interference between different intermediate mechanisms.

The process  $e^+e^- \rightarrow \omega\pi^0$  in the  $\omega \rightarrow \pi^0\gamma$  decay mode was first studied in the ND experiment [4] at the VEPP-2M collider. The cross section was measured at c.m. energies below 1.4 GeV. Later this measurement was repeated by

---

\*e-mail: l.v.kardapoltsev@inp.nsk.su

the SND [5] and CMD-2 [6] detectors with much higher statistics. In the energy region near the  $\phi$ -meson resonance the cross section was measured in the SND experiment [7] and then in the KLOE experiment [8]. Our measurement of the  $e^+e^- \rightarrow \omega\pi^0 \rightarrow \pi^0\pi^0\gamma$  cross section at VEPP-2000 based on  $5 \text{ pb}^{-1}$  collected in 2010 was published in Ref. [9].

The first measurement of the process  $e^+e^- \rightarrow \omega\pi^0$  in the  $\omega \rightarrow \pi^+\pi^-\pi^0$  decay mode was performed by the DM2 Collaboration [10]. For a long time this measurement was the only one above 1.4 GeV. Below 1.4 GeV this cross section was measured at VEPP-2M by SND [7, 11] and CMD-2 [12], and in the KLOE experiment [8] in the  $\phi$ -meson region.

## II. EXPERIMENT

SND [2] is a general purpose non-magnetic detector. Its main part is a spherical three-layer NaI(Tl) calorimeter with 560 individual crystals per layer and 90% solid angle coverage. The calorimeter energy resolution for photons is  $\sigma_E/E_\gamma = 4.2\%/\sqrt[4]{E_\gamma(\text{GeV})}$ , the angular resolution  $\simeq 1.5^\circ$ . There is a tracking system around the collider beam pipe based on a nine-layer drift chamber and a one-layer proportional chamber with cathode-strip readout. Outside the calorimeter a muon detector consisting of proportional tubes and scintillation counters is placed. An aerogel Cherenkov counter located between the drift chamber and the calorimeter is used for particle identification.

Experiments at VEPP-2000 started in 2010. During 2010–2012 the c.m. energy range  $E = 1.05\text{--}2.00$  GeV was scanned several times with a step of 20–25 MeV. The total integrated luminosity collected by SND in this energy range is about  $40 \text{ pb}^{-1}$ . This work is based on data ( $27 \text{ pb}^{-1}$ ) recorded in 2010–2011.

During the experiment, beam energy was determined using measurements of the magnetic field in the collider bending magnets. To fix the absolute energy scale, scan of the  $\phi(1020)$  resonance was performed and its mass was measured. However, possible instability and uncertainties in collider components may lead to a sizable energy bias when the beam energy increases from 0.5 to 1 GeV. The uncertainty in the energy setting was investigated in 2012 in special runs, in which the beam energy was measured using the Compton backscattering method [13]. Based on the results of these runs we conservatively estimate the uncertainty in the c.m. energy to be 5 MeV.

## III. LUMINOSITY MEASUREMENT

In this analysis the process

$$e^+e^- \rightarrow \gamma\gamma \quad (2)$$

is used for luminosity measurement. Similar to the process under study (1), the normalizing process (2) does not contain charged particles in the final state. The selection criteria for the process (2) are chosen in such a manner that some uncertainties on the cross section measurement cancel as a result of the normalization.

For example, in the selection of five-photon events of the process under study we require the absence of charged tracks in an event. This leads to loss of signal events that contain beam-generated spurious tracks. The probability of such a loss may reach several percent and strongly depends on experimental conditions (vacuum pressure in the collider beam pipe, beam currents, ...). Since the same condition is used for selection of the normalization process, the systematic uncertainty associated with beam-generated extra tracks cancels. Moreover, events of both processes are selected by the same hardware trigger. Therefore the uncertainty associated with the trigger inefficiency cancels too.

To select events of the process (2), the following selection criteria are used:

- at least two photons and no charged particles are detected,
- the number of hits in the drift chamber is less than or equal to five,
- the energies of two most energetic photons in an event are larger than  $0.3E$ ,
- the azimuth angles of these photons satisfy the condition  $|\phi_1 - \phi_2 - 180^\circ| < 11.5^\circ$ ,
- the polar angles of these photons satisfy the conditions  $|\theta_1 + \theta_2 - 180^\circ| < 17.2^\circ$  and  $36^\circ < \theta_{1,2} < 144^\circ$ .

Photons are reconstructed as clusters in the electromagnetic calorimeter with energies greater than 30 MeV not associated with charged tracks in the drift chamber.

The condition on the number of hits suppresses background from Bhabha events with unreconstructed tracks in the drift chambers. We do not expect any significant background from other  $e^+e^-$  annihilation processes in the energy

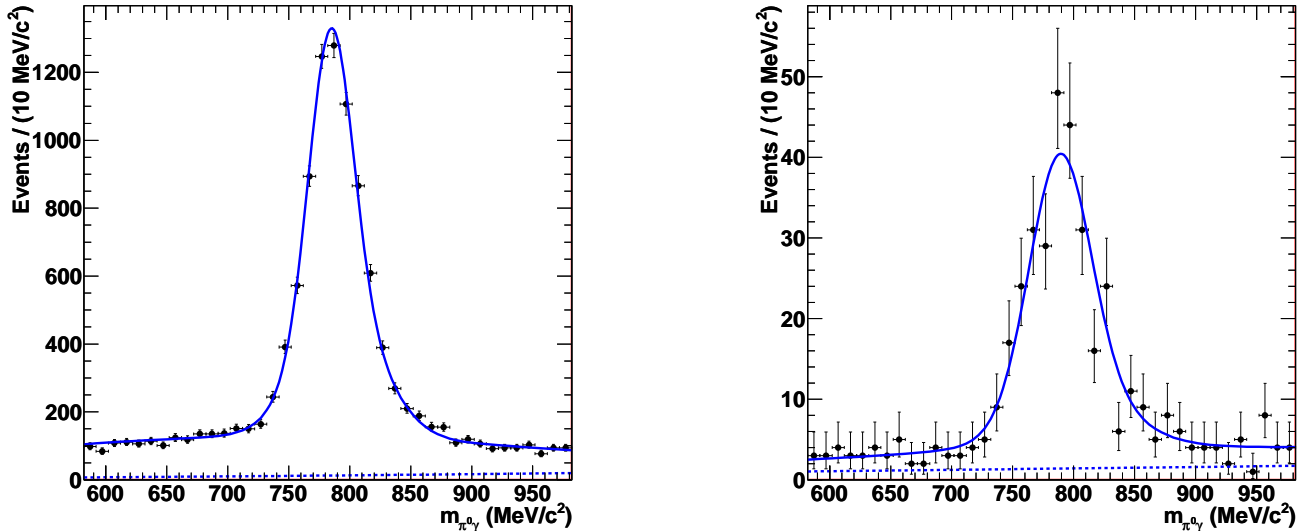


FIG. 1: The distribution of the  $\pi^0\gamma$  invariant mass for selected data events (points with error bars) with  $E < 1.7$  GeV (left) and  $E \geq 1.7$  GeV (right). The curves are the result of the fit described in the text. The dashed line represents the linear-background contribution.

region under study. To estimate possible cosmic-ray background, data recorded during 7.5 hours in a special run without beams are analyzed. No  $e^+e^- \rightarrow \gamma\gamma$  candidates are selected. We estimate that the fraction of cosmic events in the sample of selected two-photon events is less than  $2 \times 10^{-4}$  and conclude that the cosmic-ray background is negligible.

To calculate the detection efficiency and the cross section of the process (2), a Monte-Carlo (MC) event generator based on Ref. [14] is used. The integrated luminosity measured for each energy point is listed in Table I. The theoretical uncertainty on the cross section calculation is about 1%. The systematic uncertainty on the detection efficiency is estimated to be 2%.

#### IV. EVENT SELECTION

At the first stage of the analysis, five-photon events are selected with following criteria:

- at least five photons and no charged particles are detected,
- the number of hits in the drift chamber is less than or equal to five,
- $E_{tot}/E > 0.5$ , where  $E_{tot}$  is the total energy deposition in the calorimeter.

For events passing the preliminary selection, kinematic fits to the  $e^+e^- \rightarrow 5\gamma$  and  $e^+e^- \rightarrow \pi^0\pi^0\gamma$  hypotheses are performed with requirements of energy and momentum conservation and  $\pi^0$  mass constraints for the second hypothesis. The goodness of the fits is characterized by the  $\chi^2$  parameters:  $\chi_{5\gamma}^2$  and  $\chi_{\pi^0\pi^0\gamma}^2$ . For events with more than five photons, all five-photon combinations are tested and the one with minimal  $\chi_{\pi^0\pi^0\gamma}^2$  is used. To select  $\omega\pi^0$  candidates the following additional conditions are applied:

- $\chi_{5\gamma}^2 < 30$  for  $E < 1.7$  GeV and  $\chi_{5\gamma}^2 < 15$  for  $E \geq 1.7$  GeV,
- $\chi_{\pi^0\pi^0\gamma}^2 - \chi_{5\gamma}^2 < 10$ ,
- at least one of the two  $\pi^0\gamma$  invariant masses satisfies the condition  $|m_{\pi^0\gamma} - M_\omega| < 200$  MeV/ $c^2$ , where  $M_\omega$  is the  $\omega$ -meson nominal mass [15].

The distributions of the  $\pi^0\gamma$  invariant mass for 7899 selected data events at  $E < 1.7$  GeV and 331 data events at  $E \geq 1.7$  GeV are shown in Fig. 1. The  $\omega$  meson peak is clearly seen in both distributions. Since each event has two entries into the histogram, the nonresonant parts of the distributions are determined mainly by signal events.

## V. FITTING THE $\pi^0\gamma$ MASS SPECTRA

To determine the number of signal events, the  $\pi^0\gamma$  mass spectrum is fitted by a sum of signal ( $F_s$ ) and background ( $F_b$ ) distributions. The signal distribution is obtained by fitting the mass spectrum for simulated signal events with a non-parametric kernel estimation technique [16]. To take into account a difference between data and MC simulation in mass resolution and calibration, the  $\pi^0\gamma$  mass for simulated events is smeared and shifted before the fit. The values of the smearing Gaussian sigma ( $\sigma_s$ ) and mass shift ( $\Delta m$ ) are deduced from comparison of the  $\omega$  peak width and position in data with the same parameters in simulation. To study energy dependence of  $\sigma_s$  and  $\Delta m$ , comparison is performed in three c.m. energy regions below 1.7 GeV. The mass shift and the Gaussian sigma are found to be linearly dependent on the energy. The value of  $\Delta m$  changes from  $(1.0 \pm 0.5)$  MeV/ $c^2$  in the energy region 1.05–1.30 GeV to  $(3.9 \pm 0.5)$  MeV/ $c^2$  in the energy region 1.5–1.7 GeV. The value of  $\sigma_s$  for the same energy regions changes from  $(6.2 \pm 1.0)$  MeV/ $c^2$  to  $(10.5 \pm 0.5)$  MeV/ $c^2$ . For energies above 1.7 GeV, where statistics are small,  $\sigma_s$  is obtained by a linear extrapolation from lower energies.

The main sources of background are QED processes such as  $e^+e^- \rightarrow 3\gamma, 4\gamma, 5\gamma$ , and the hadronic processes  $e^+e^- \rightarrow \eta\gamma$  and  $e^+e^- \rightarrow \omega\pi^0\pi^0$ . Background can arise also from the process  $e^+e^- \rightarrow \pi^0\pi^0\gamma$  with intermediate states other than the  $\omega\pi^0$ , for example,  $f_2\gamma$ . The  $\pi^0\gamma$  mass distribution for the QED,  $\eta\gamma$  and  $\pi^0\pi^0\gamma$  events is expected to be flat and is described by a linear function. The distribution for  $\omega\pi^0\pi^0$  events obtained from MC simulation has a complex shape with a wide maximum shifted to the right of the  $\omega$  peak position. The expected number of  $\omega\pi^0\pi^0$  events is calculated using experimental data on the  $e^+e^- \rightarrow \omega\pi^+\pi^-$  cross section [17] and the isotopic relation  $\sigma(\omega\pi^+\pi^-) = 2\sigma(\omega\pi^0\pi^0)$ . The background from  $e^+e^- \rightarrow \omega\pi^0\pi^0$  is important in the energy range 1.7–1.9 GeV, but even there it does not exceed 6% of signal.

The cross section for the process  $e^+e^- \rightarrow \rho^0\pi^0 \rightarrow \pi^0\pi^0\gamma$  is estimated from the  $e^+e^- \rightarrow \rho\pi \rightarrow 3\pi$  cross section measured by BABAR [18], and found to be small, below 1 pb. However, because of closeness of the  $\rho$  and  $\omega$  masses, the interference between the  $\omega\pi^0$  and  $\rho^0\pi^0$  amplitudes can give a sizable contribution to the measured  $e^+e^- \rightarrow \omega\pi^0 \rightarrow \pi^0\pi^0\gamma$  cross section. The  $\pi^0\gamma$  spectrum for the interference term is peaked at  $\omega$  mass and practically indistinguishable from the spectrum for the  $\omega\pi^0$  intermediate state. Since the phase between  $\omega\pi^0$  and  $\rho^0\pi^0$  amplitudes is unknown, we calculate the maximum possible value of the interference term and use this value as an estimate of the systematic uncertainty on the measured  $\omega\pi^0$  cross section. The uncertainty due to the interference is estimated to be 2% at  $E \leq 1.55$  GeV, then increases to 4.5% at 1.7 GeV, and to 8.0% at 1.8 GeV. Above 1.8 GeV this uncertainty is negligible in comparison with the uncertainty of the radiative correction.

To determine the number of signal events we perform an unbinned extended likelihood fit to the mass spectrum in the range  $|m_{\pi^0\gamma} - M_\omega| < 200$  MeV/ $c^2$ . The likelihood function used for  $E < 1.7$  GeV is given as follows:

$$L = P_P(N; N_s + N_b) P_B(M - N; N, k_t) \prod_{i=1}^M \left( F_s(m_{\pi^0\gamma}^i) \frac{N_s(1 + k_s)}{N_s(1 + k_s) + N_b(1 + k_b)} + F_b(m_{\pi^0\gamma}^i) \frac{N_b(1 + k_b)}{N_s(1 + k_s) + N_b(1 + k_b)} \right) \quad (3)$$

where  $N$  is the number of selected events,  $M$  is the total number of entries in the fitted spectrum,  $N_s$  ( $N_b$ ) is the numbers of signal (background) events,  $k_s$  ( $k_b$ ) is the fraction of signal (background) events with two entries per event, i.e. events for which masses of both  $\pi^0\gamma$  combinations satisfy the condition  $|m_{\pi^0\gamma} - M_\omega| < 200$  MeV/ $c^2$ ,  $k_t = (N_s k_s + N_b k_b) / (N_s + N_b)$ . The functions  $P_P$  and  $P_B$  are Poisson and binomial distributions for the total number of selected events and the number of selected events with two entries to the fitted spectrum, respectively. The parameter  $k_s$  is calculated using signal MC simulation. It changes from 0.4 at  $E = 1.1$  GeV to 0.2 at  $E = 2.0$  GeV. To understand the range of  $k_b$  variation, we use MC simulation of the  $e^+e^- \rightarrow \pi^0\pi^0\gamma$  events at the generator level in different models: according to phase space, with the intermediate  $f_0(980)\gamma$ ,  $f_2(1270)\gamma$ , and  $f_0(1370)\gamma$  states. In the energy range under study the  $k_b$  value is found to change from 0.1 to 0.5. Therefore, the parameter  $k_b$  is set to be  $0.3 \pm 0.2$  in the fit (the likelihood function is multiplied by the corresponding Gaussian). The background distribution  $F_b$  is described by a linear function. Above 1.7 GeV a term describing  $\omega\pi^0\pi^0$  contribution is added into the likelihood function.

The fit results are shown in Fig. 1. To obtain the shape of the mass spectrum for signal, the distribution of simulated events over energy points is weighted to yield the distribution observed in data. It is seen that our model for signal and background describes well the experimental mass spectra. The total numbers of signal and background events are  $7533 \pm 110$  and  $366 \pm 70$ , respectively, for  $E < 1.7$  GeV, and  $282 \pm 22$  and  $49 \pm 15$  for  $E \geq 1.7$  GeV. A similar fitting procedure is applied in each energy point. The numbers of signal events obtained from the fits are listed in Table I.

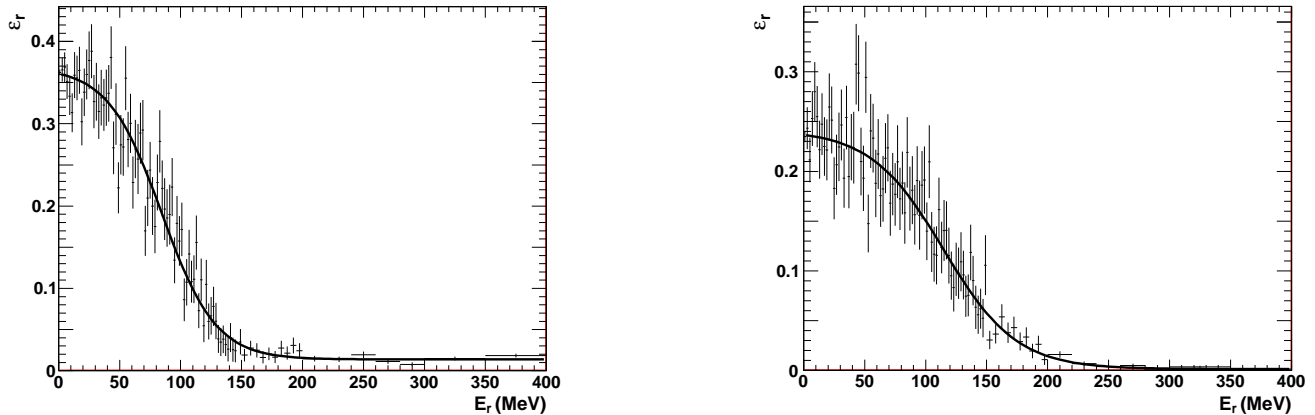


FIG. 2: The  $E_r$  dependence of the detection efficiency for the process  $e^+e^- \rightarrow \omega\pi^0 \rightarrow \pi^0\pi^0\gamma$  for  $E = 1.05$  GeV (left) and  $E = 2.00$  GeV (right).

## VI. DETECTION EFFICIENCY AND RADIATIVE CORRECTIONS

The detection efficiency for the process under study is determined using MC simulation. The simulation includes radiative corrections to the Born cross section calculated according to Ref. [19]. In particular, an extra photon emitted by initial electrons is generated with the angular distribution modeled according to Ref. [20]. The detection efficiency  $\varepsilon_r$  is evaluated as a function of two parameters: the c.m. energy  $E$  and the energy of the extra photon  $E_r$ . The  $E_r$  dependence of the detection efficiency is shown in Fig. 2 for the energy points with minimum and maximum energies studied.

The visible cross section for the process  $e^+e^- \rightarrow \omega\pi^0 \rightarrow \pi^0\pi^0\gamma$  is written as

$$\sigma_{vis} = \int_0^{x_{max}} \varepsilon_r(E, xE/2) F(x, E) \sigma(E\sqrt{1-x}) dx, \quad (4)$$

where  $\sigma(E)$  is the Born cross section, which one needs to extract from the experiment,  $F(x, E)$  is a function describing the probability to emit extra photons with the total energy  $xE/2$  [19]. Equation (4) can be rewritten in the conventional form:

$$\sigma_{vis} = \varepsilon(E) \sigma(E) (1 + \delta(E)), \quad (5)$$

where  $\delta(E)$  is the radiative correction, and  $\varepsilon(E)$  is defined as follows:

$$\varepsilon(E) \equiv \varepsilon_r(E, 0). \quad (6)$$

Technically the determination of the Born cross section is performed as follows. With the use of Eq. (4) the energy dependence of the measured visible cross section is approximated. To do this the Born cross section is parametrized by some theoretical model that describes data reasonably well. The fitted model parameters are used to evaluate the radiative correction  $\delta(E)$ . Then the experimental values of the Born cross section are obtained using Eq.(5). To estimate the model dependence of the radiative correction, the model parameters are varied in a wide range, with the condition that the approximation quality remains acceptable. The fit to the measured cross section is described in detail in Sec. VII. The obtained values of the radiative correction are listed in Table I. The systematic uncertainty associated with the radiative corrections is estimated to be about 1% at  $E < 1.6$  GeV and increases up to 5% at  $E = 1.7$  GeV. Above 1.7 GeV the radiative correction becomes large and highly model dependent. For these energy points we quote a range of  $(1 + \delta)$  variation.

Imperfect simulation of detector response for photons leads to a systematic uncertainty in the detection efficiency. To estimate this uncertainty, the data distributions of the most important selection parameters  $\chi_{5\gamma}^2$  and  $(\chi_{\pi^0\pi^0\gamma}^2 - \chi_{5\gamma}^2)$  for signal events are compared with corresponding simulated distributions. The distributions are shown in Fig. 3 for events with  $E < 1.7$  GeV. They are normalized to the same number of events. The distributions for background events shown in Fig. 3 by the shaded histograms are obtained using data from the  $m_{\pi^0\gamma}$  sideband ( $66.7 \text{ MeV}/c^2 < |m_{\pi^0\gamma} - M_\omega| < 200.0 \text{ MeV}/c^2$ ). These background distributions are added to the simulated signal distributions.

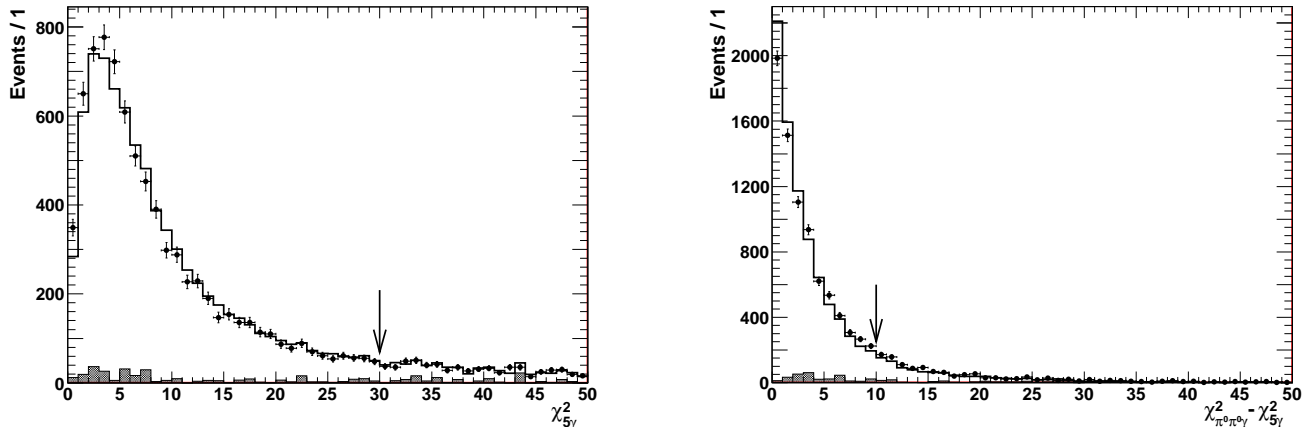


FIG. 3: The  $\chi^2_{5\gamma}$  (left) and  $(\chi^2_{\pi^0\pi^0\gamma} - \chi^2_{5\gamma})$  (right) distributions for data events with  $E < 1.7$  GeV (points with error bars). The open histogram is a sum of the simulated signal distribution and background distribution. The latter is shown by the shaded histogram. The data and the signal+background distributions are normalized to the same number of events. The arrows indicate the selection criteria used.

A difference between data and MC simulation is seen in both the distributions. To obtain numerical estimation, we change the limits of the conditions on  $\chi^2_{5\gamma}$  and  $(\chi^2_{\pi^0\pi^0\gamma} - \chi^2_{5\gamma})$  from 30 to 50 and from 10 to 50, respectively. The resulting variation of the measured cross section  $\delta\sigma_{\omega\pi}$  is found to be  $(-0.4 \pm 0.5)\%$  for the  $\chi^2_{5\gamma}$  condition, and  $(2.9 \pm 0.5)\%$  for the  $(\chi^2_{\pi^0\pi^0\gamma} - \chi^2_{5\gamma})$  condition. The obtained values of  $\delta\sigma_{\omega\pi}$  are used to calculate a correction to the detection efficiency. The detection efficiency obtained from simulation for our standard selection criteria should be decreased by  $(-2.5 \pm 0.7)\%$ .

In the SND a photon converted in material before the drift chamber produces a track. Events with converted photons are rejected by the selection criteria used. Since the numbers of photons in the final state are different for the signal and normalization processes, the data-MC simulation difference in the conversion probability leads to a systematic shift in the measured cross section. The conversion probability is measured using  $\phi \rightarrow \eta\gamma \rightarrow 3\gamma$  events collected in a special run in vicinity of the  $\phi$ -meson resonance and is found to be  $(0.97 \pm 0.28)\%$  in data and  $(0.78 \pm 0.04)\%$  in simulation. The data-MC simulation difference  $(0.19 \pm 0.28)\%$  is consistent with zero. We conclude that the simulation reproduces the photon conversion reasonably well. The statistical error (0.3%) of the data-MC simulation difference is taken as an estimate of the systematic uncertainty on the photon conversion. The corresponding uncertainty on the measured cross section is estimated as  $3 \times 0.3 = 0.9\%$  (the contributions from two of five photons cancel due to normalization).

As it was discussed earlier, some part of the data events contains beam-generated spurious tracks and photons. The effect of extra tracks cancels due to normalization to two-photon events. The presence of extra photons also changes the detection efficiency, but differently for the signal and normalization processes. To take into account this effect in MC simulation, beam-background events recorded during experiment with a special random trigger are merged with simulated events. The detection efficiencies obtained using simulation with and without merged background are compared. It is found that the presence of extra photons does not influence the number of selected normalization events. The detection efficiency for the signal process increases by 0.3–1.3% depending on experimental conditions. Unfortunately, the random-trigger events were not recorded on a regular basis during the 2010–2011 experiments. Therefore, we conservatively estimate the correction due to extra photons to the signal detection efficiency to be 0.8% with a systematic uncertainty of 0.5%.

The corrected values of the detection efficiency  $\varepsilon(E)$  are listed in Table I. The statistical error on the detection efficiency is negligible. A systematic uncertainty from the sources discussed above is 1.2%. A nonmonotonic behavior of  $\varepsilon(E)$  as a function of the c.m. energy is due to variations of experimental conditions, in particular, due to dead calorimeter channels, a fraction of which changed from 2.4% to 3.4% during the data taking period.

## VII. RESULTS AND DISCUSSION

The Born cross section for  $e^+e^- \rightarrow \omega\pi^0 \rightarrow \pi^0\pi^0\gamma$  obtained using Eq.(5) is shown in Fig. 4 in comparison with the results of previous measurements. The numerical values are listed in Table I. The quoted errors on the cross section

TABLE I: The c.m. energy ( $E$ ), integrated luminosity ( $IL$ ), detection efficiency ( $\varepsilon$ ), number of selected signal events ( $N_s$ ), radiative-correction factor ( $1 + \delta$ ), measured Born cross section ( $\sigma$ ). For the cross section the first error is statistical, the second is systematic.

| $E$ , GeV | $IL$ , nb $^{-1}$ | $\varepsilon$ , % | $N_s$           | $1 + \delta$ | $\sigma$ , nb                          |
|-----------|-------------------|-------------------|-----------------|--------------|----------------------------------------|
| 1.050     | 358               | 35.5              | 104 ± 11        | 0.903        | 0.90 ± 0.10 ± 0.03                     |
| 1.075     | 545               | 36.5              | 176 ± 15        | 0.913        | 0.97 ± 0.08 ± 0.03                     |
| 1.100     | 845               | 36.0              | 297 ± 17        | 0.921        | 1.06 ± 0.06 ± 0.04                     |
| 1.125     | 518               | 35.9              | 220 ± 16        | 0.928        | 1.28 ± 0.09 ± 0.04                     |
| 1.150     | 412               | 37.8              | 178 ± 13        | 0.934        | 1.23 ± 0.09 ± 0.04                     |
| 1.175     | 539               | 36.8              | 231 ± 17        | 0.939        | 1.24 ± 0.09 ± 0.04                     |
| 1.200     | 1058              | 36.6              | 489 ± 24        | 0.943        | 1.34 ± 0.06 ± 0.05                     |
| 1.225     | 550               | 37.8              | 265 ± 19        | 0.947        | 1.35 ± 0.10 ± 0.05                     |
| 1.250     | 435               | 37.9              | 187 ± 17        | 0.950        | 1.19 ± 0.11 ± 0.04                     |
| 1.275     | 495               | 37.0              | 254 ± 21        | 0.953        | 1.46 ± 0.12 ± 0.05                     |
| 1.300     | 1278              | 37.6              | 673 ± 35        | 0.956        | 1.47 ± 0.08 ± 0.05                     |
| 1.325     | 522               | 38.2              | 279 ± 24        | 0.959        | 1.46 ± 0.12 ± 0.05                     |
| 1.350     | 554               | 38.1              | 292 ± 24        | 0.962        | 1.44 ± 0.12 ± 0.05                     |
| 1.375     | 574               | 38.1              | 302 ± 24        | 0.966        | 1.43 ± 0.11 ± 0.05                     |
| 1.400     | 1012              | 37.9              | 578 ± 33        | 0.970        | 1.55 ± 0.09 ± 0.05                     |
| 1.425     | 598               | 38.1              | 363 ± 26        | 0.977        | 1.63 ± 0.12 ± 0.05                     |
| 1.450     | 427               | 38.3              | 221 ± 19        | 0.985        | 1.37 ± 0.12 ± 0.05                     |
| 1.475     | 599               | 38.4              | 291 ± 21        | 0.995        | 1.27 ± 0.09 ± 0.04                     |
| 1.500     | 1939              | 39.0              | 996 ± 40        | 1.007        | 1.31 ± 0.05 ± 0.04                     |
| 1.525     | 487               | 38.2              | 245 ± 19        | 1.021        | 1.29 ± 0.10 ± 0.05                     |
| 1.550     | 543               | 38.2              | 228 ± 16        | 1.038        | 1.06 ± 0.08 ± 0.04                     |
| 1.575     | 505               | 37.9              | 170 ± 17        | 1.063        | 0.83 ± 0.08 ± 0.04                     |
| 1.600     | 814               | 38.1              | 232 ± 19        | 1.100        | 0.68 ± 0.06 ± 0.03                     |
| 1.625     | 505               | 37.9              | 139 ± 15        | 1.161        | 0.63 ± 0.07 $^{+0.03}_{-0.04}$         |
| 1.650     | 473               | 36.9              | 96 ± 10         | 1.262        | 0.44 ± 0.04 $^{+0.02}_{-0.03}$         |
| 1.675     | 454               | 37.0              | 74 ± 11         | 1.429        | 0.31 ± 0.05 $^{+0.01}_{-0.02}$         |
| 1.700     | 698               | 30.3              | 70 ± 10         | 1.704        | 0.19 ± 0.05 $^{+0.01}_{-0.01}$         |
| 1.725     | 502               | 30.6              | 22 ± 6          | 2.0–2.3      | 0.06 ± 0.04 $^{+0.007}_{-0.006}$       |
| 1.750     | 503               | 29.2              | 25 ± 6          | 2.4–3.3      | 0.06 ± 0.04 $^{+0.02}_{-0.01}$         |
| 1.775     | 521               | 28.7              | 22 ± 6          | 2.8–5.0      | 0.03 ± 0.04 $^{+0.02}_{-0.01}$         |
| 1.800     | 727               | 27.9              | 33 ± 7          | 3.4–9.0      | 0.02 ± 0.04 $^{+0.02}_{-0.005}$        |
| 1.825     | 477               | 28.2              | 7 ± 3           | 4–15         | 0.004 $^{+0.027+0.008}_{-0.022-0.0}$   |
| 1.850     | 400               | 26.7              | 4 $^{+4}_{-3}$  | 5–24         | 0.002 $^{+0.037+0.005}_{-0.027-0.0}$   |
| 1.870     | 631               | 26.2              | 19 ± 6          | 5–27         | 0.005 $^{+0.038+0.016}_{-0.033-0.0}$   |
| 1.890     | 577               | 26.3              | 24 ± 5          | 6–31         | 0.006 $^{+0.034+0.022}_{-0.031-0.001}$ |
| 1.900     | 553               | 24.9              | 12 $^{+4}_{-5}$ | 6–40         | 0.004 $^{+0.028+0.011}_{-0.038-0.002}$ |
| 1.925     | 555               | 24.6              | 14 $^{+4}_{-3}$ | 5–68         | 0.006 $^{+0.030+0.013}_{-0.025-0.005}$ |
| 1.950     | 406               | 23.3              | 1 $^{+2}_{-1}$  | 5–63         | 0.001 $^{+0.021+0.001}_{-0.013-0.001}$ |
| 1.975     | 460               | 24.0              | 9 $^{+4}_{-5}$  | 5–39         | 0.009 $^{+0.033+0.008}_{-0.041-0.007}$ |
| 2.000     | 536               | 23.3              | 5 $^{+3}_{-2}$  | 4–39         | 0.006 $^{+0.024+0.005}_{-0.018-0.005}$ |

are statistical and systematic. The sources of systematic uncertainty are summarized in Table II. The total systematic uncertainty is 3.4% in the energy range  $E \leq 1.55$  GeV and 4.5% in the energy range  $1.55 < E < 1.6$ . Above 1.6 GeV the uncertainty increases due to the model dependence of the radiative correction.

Our data are in good agreement with the measurements [5, 6] performed by SND and CMD-2 at the VEPP-2M collider at energies below 1.4 GeV, but significantly (by 20–30%) exceed the DM2 data [10]. The DM2 data were obtained in the  $\pi^+\pi^-\pi^0\pi^0$  mode and have been rescaled using the ratio of the  $\omega \rightarrow \pi^0\gamma$  and  $\omega \rightarrow 3\pi$  decay probabilities [15].

The cross section measured in this work is fitted together with the SND data obtained in experiments at VEPP-2M [5]. The Born cross section is described by the following formula [5]

$$\sigma(E) = \frac{4\pi\alpha^2}{E^3} \left( \frac{g_{\rho\omega\pi}}{f_\rho} \right)^2 \left| \frac{m_\rho^2}{D_\rho} + A_1 e^{i\phi_1} \frac{m_{\rho'}^2}{D_{\rho'}} + A_2 e^{i\phi_2} \frac{m_{\rho''}^2}{D_{\rho''}} + A_3 \frac{m_{\rho'''}^2}{D_{\rho'''}} \right|^2 P_f(E) B(\omega \rightarrow \pi^0\gamma), \quad (7)$$

where  $\alpha$  is the fine structure constant,  $g_{\rho\omega\pi}$  is the  $\rho \rightarrow \omega\pi$  coupling constant,  $f_\rho$  is the  $\gamma^* \rightarrow \rho$  coupling constant

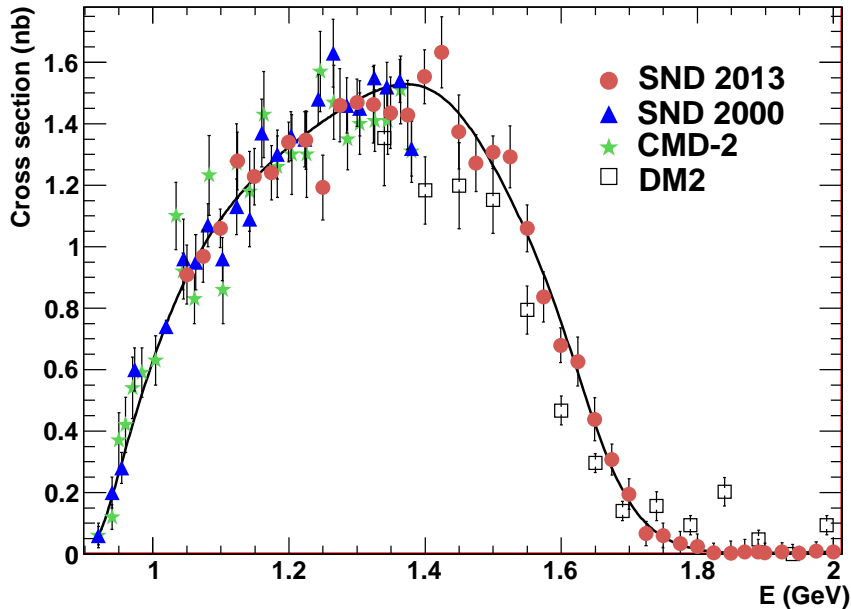


FIG. 4: The cross section for  $e^+e^- \rightarrow \omega\pi^0 \rightarrow \pi^0\pi^0\gamma$  measured in this work (circles), and in SND [5] (triangles), CMD-2 [6] (stars), and DM2 [10] (squares) experiments. Only statistical errors are shown. The curve is the result of the fit to SND 2000 and SND 2013 data described in the text.

TABLE II: The systematic uncertainties on the measured cross section from different sources and the correction to the detection efficiency. The total uncertainty is the sum of all the contributions in quadrature.

| Source                                           | Systematic uncertainty, % | Correction, % |
|--------------------------------------------------|---------------------------|---------------|
| Luminosity                                       | 2.2                       | —             |
| Selection criteria                               | 0.7                       | -2.5          |
| Photon conversion                                | 0.9                       | —             |
| Beam background                                  | 0.5                       | 0.8           |
| Radiative correction ( $E < 1.6$ GeV)            | 1                         | —             |
| Interference with $\rho^0\pi^0$ ( $E < 1.6$ GeV) | 2-3.6                     | —             |
| Total                                            | 3.4-4.5                   | -1.7          |

calculated from the  $\rho \rightarrow e^+e^-$  decay width,  $D_{\rho_i}(E) = m_{\rho_i}^2 - E^2 - iE\Gamma_{\rho_i}(E)$ ,  $m_{\rho_i}$  and  $\Gamma_{\rho_i}(E)$  are the mass and width of the resonance  $\rho_i$ ,  $B(\omega \rightarrow \pi^0\gamma)$  is the  $\omega \rightarrow \pi^0\gamma$  branching fraction. The first term in Eq. (7) describes the contribution of the  $\rho(770)$  resonance, the second and third represent the  $\rho(1450)$  and  $\rho(1700)$  contributions. The fourth term is added to study a model dependence of the measured cross section due to possible existence of a broad  $\rho$ -like resonance with mass  $m_{\rho''} > 2$  GeV/ $c^2$  or due to nonresonant contribution into the Born cross section near 2 GeV. The parameters  $A_i$  are the ratios of the coupling constants  $A_i = g_{\rho_i\omega\pi}/g_{\rho\omega\pi} \cdot f_{\rho}/f_{\rho_i}$ ,  $\phi_1$  and  $\phi_2$  are the phases of the  $\rho(1450)$  and  $\rho(1700)$  amplitudes relative to the  $\rho(770)$  amplitude. For  $\rho'''$  contribution, the phase is assumed to be equal to zero. The energy dependence of the phase-space factor  $P_f(E)$  is calculated using the MC event generator for signal events. For an infinitely narrow  $\omega$  resonance,  $P_f(E) = 1/3 \cdot q_\omega^3$ , where  $q_\omega$  is the  $\omega$  meson momentum. The energy dependence of the  $\rho(770)$  width is described as follows:

$$\Gamma_\rho(E) = \Gamma_\rho(m_\rho) \left(\frac{m_\rho}{E}\right)^2 \left(\frac{q_\pi(E)}{q_\pi(m_\rho)}\right)^3 + \frac{g_{\rho\omega\pi}^2}{12\pi} q_\omega^3, \quad (8)$$

where  $q_\pi(E) = \sqrt{(E/2)^2 - m_\pi^2}$ ,  $m_\pi$  is the  $\pi^-$  mass. For  $\rho(1450)$  and  $\rho(1700)$ , the energy-independent widths are used.

The data are fit with free parameters  $g_{\rho\omega\pi}$ ,  $A_1$ ,  $A_2$ ,  $A_3$ ,  $M_{\rho'}$ ,  $M_{\rho''}$ ,  $\phi_1$ , and  $\phi_2$ . The values of the  $\rho'$  and  $\rho''$  widths are fixed at PDG values [15]:  $\Gamma_{\rho'} = 400$  MeV,  $\Gamma_{\rho''} = 250$  MeV. The parameters  $M_{\rho'''}$  and  $\Gamma_{\rho'''}$  are set to 2.3 GeV

TABLE III: Fit parameters obtained.

| Parameter                               | Model 1           | Model 2          |
|-----------------------------------------|-------------------|------------------|
| $g_{\rho\omega\pi}$ , $\text{GeV}^{-1}$ | $15.6 \pm 0.3$    | $17.4 \pm 0.1$   |
| $A_1$                                   | $0.26 \pm 0.01$   | $0.11 \pm 0.001$ |
| $A_2$                                   | $0.060 \pm 0.006$ | $\equiv 0$       |
| $M_{\rho'}$ , MeV                       | $1491 \pm 19$     | $1488 \pm 3$     |
| $\Gamma_{\rho'}$ , MeV                  | $\equiv 400$      | $321 \pm 4$      |
| $M_{\rho''}$ , MeV                      | $1708 \pm 41$     | —                |
| $\Gamma_{\rho''}$ , MeV                 | $\equiv 250$      | —                |
| $\phi_1$ , deg.                         | $168 \pm 3$       | $121 \pm 2$      |
| $\phi_2$ , deg.                         | $10 \pm 7$        | —                |
| $\chi^2/\nu$                            | $56.8 / 52$       | $118.6 / 54$     |

and 400 MeV, respectively. The fit result is shown in Fig. 4. The fitted parameters are used to calculate the values of the radiative corrections listed in Table I. To estimate the model dependence of the radiative correction, the fit is performed with  $M_{\rho'}$  fixed at different values from the range 1.4–1.6 GeV and with  $A_3$  either free or fixed at zero. The quality  $P(\chi^2; \nu)$  of these fits, where  $\nu$  is the number of degrees of freedom, varies from 5 to 20%.

To study the contributions of the  $\rho(1450)$  and  $\rho(1700)$  resonances, we restrict the energy range to  $E \leq 1.9$  GeV. This reduces the model uncertainty due to a possible nonresonant contribution or the  $\rho'''$  resonance. The parameter  $A_3$  is set to zero. The fit results are presented in Table III. Two models have been studied, with a non-zero and zero  $\rho''$  contribution. In the fit with the second model the parameter  $\Gamma_{\rho'}$  is left free. Such a fit with only one  $\rho$  excitation was performed in Ref. [6] and gave a reasonable description of CMD-2 and DM2 data. It is seen that our more precise data cannot be described by the model with one excited  $\rho$  state. The fitted value of the parameter  $A_i$  is used to calculate the products of the branching fractions

$$B(\rho_i \rightarrow \omega\pi^0) \cdot B(\rho_i \rightarrow e^+e^-) = \frac{\sigma_{\rho_i}(m_{\rho_i})m_{\rho_i}^2}{12\pi}, \quad (9)$$

where

$$\sigma_{\rho_i}(E) = \frac{4\pi\alpha^2}{E^3} \left( \frac{g_{\rho\omega\pi}}{f_\rho} \right)^2 \left| A_i \frac{m_{\rho_i}^2}{D_{\rho_i}} \right|^2 P_f(E) \quad (10)$$

is the cross section for the process  $e^+e^- \rightarrow \rho_i \rightarrow \omega\pi^0$  without interference with other  $\rho$ -like resonances. The results are following

$$\begin{aligned} B(\rho' \rightarrow e^+e^-) \cdot B(\rho' \rightarrow \omega\pi^0) &= (5.3 \pm 0.4) \times 10^{-6}, \\ B(\rho'' \rightarrow e^+e^-) \cdot B(\rho'' \rightarrow \omega\pi^0) &= (1.7 \pm 0.4) \times 10^{-6}. \end{aligned} \quad (11)$$

It should be noted that at the moment there is no generally accepted approach for describing the tail of the  $\rho(770)$  resonance above 1 GeV and shapes of broad resonances like  $\rho'$  and  $\rho''$ . The excitation curves of the three resonances  $\rho$ ,  $\rho'$  and  $\rho''$  overlap; their amplitudes strongly interfere with each other. As a result, a small change of the resonance shape can lead to significant shifts in fitted resonance parameters. So, the results obtained with our very simple model using energy-independent  $\rho'$  and  $\rho''$  widths can be considered only as rough estimates of the resonance parameters.

The cross section for  $e^+e^- \rightarrow \omega\pi^0$  can be expressed in terms of the  $\gamma^* \rightarrow \omega\pi^0$  transition form factor  $F_{\omega\pi\gamma}(q^2)$  [21, 22], where  $q$  is the four-momentum of the virtual photon:

$$\sigma_{\omega\pi^0}(E) = \frac{4\pi\alpha^2}{E^3} |F_{\omega\pi\gamma}(E^2)|^2 P_f(E). \quad (12)$$

This form factor is also measured in the  $\omega \rightarrow \pi^0 e^+ e^-$  [23, 24] and  $\omega \rightarrow \pi^0 \mu^+ \mu^-$  [25, 26] decays. The value of the form factor at  $q^2 = 0$  is related to the  $\omega \rightarrow \pi^0 \gamma$  partial width:

$$\Gamma(\omega \rightarrow \pi^0 \gamma) = \frac{\alpha}{3} P_\gamma^3 |F_{\omega\pi\gamma}(0)|^2, \quad (13)$$

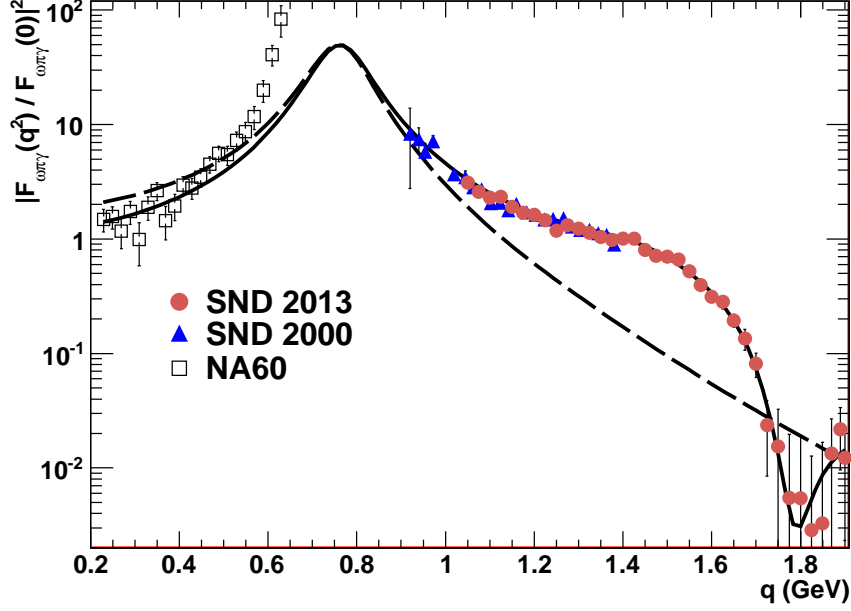


FIG. 5: The  $\gamma^* \rightarrow \omega\pi^0$  transition form factor. The points with error bars represent data from this work (circles), Ref. [5] (triangles), and Ref. [26] (squares). Only statistical errors are shown. The curve represent the result of model prediction with the parameters listed in Table III for the model 1. The dashed curve shows the  $\rho(770)$  contribution.

where  $P_\gamma$  is the decay photon momentum. Using Eqs. (7), (12), (13), and data from Table III we calculate  $\Gamma(\omega \rightarrow \pi^0\gamma)$  for the model 1 to be  $0.88 \pm 0.05$  MeV. For such a simple model the agreement with the experimental value  $\Gamma(\omega \rightarrow \pi^0\gamma) = 0.703 \pm 0.024$  MeV [15] looks reasonable.

Figure 5 shows the normalized transition form factor squared ( $|F_{\omega\pi\gamma}(q^2)/F_{\omega\pi\gamma}(0)|^2$ ) measured in this work and in Ref. [5] together with most precise data from omega decays obtained in the NA60 experiment [26]. The curve represents the results of the model prediction with the parameters listed in Table III for model 1. The dashed curve shows the  $\rho(770)$  contribution. We conclude that it is hard to describe data from  $e^+e^-$  annihilation and the  $\omega \rightarrow \pi^0\mu^+\mu^-$  decay simultaneously with our model based on vector meson dominance (VMD).

The conserved vector current (CVC) hypothesis establishes a relation between the charged hadronic current in the  $\tau$  decay and the isovector part of the electromagnetic current. So, the  $e^+e^- \rightarrow \omega\pi^0$  cross section can be related with the spectral function of the  $\tau^- \rightarrow \omega\pi^-\nu_\tau$  decay ( $V_{\omega\pi}$ ) [3]:

$$\sigma_{\omega\pi^0}(E) = \frac{4\pi^2\alpha^2}{E^2} V_{\omega\pi}(E). \quad (14)$$

The comparison of the  $e^+e^- \rightarrow \omega\pi^0 \rightarrow \pi^0\pi^0\gamma$  cross section measured by SND with the cross section calculated under the CVC hypothesis from the  $\tau^- \rightarrow \omega\pi^-\nu_\tau$  spectral function measured in the CLEO experiment [27] is presented in Fig. 6. It is seen that the  $e^+e^-$  and  $\tau$  data are in reasonable agreement. The  $\chi^2/\nu$  ( $\nu$  is the number of degrees of freedom) of comparison between the CLEO data and our fitted curve is 19.7/16. To calculate this  $\chi^2$ , a 5% systematic uncertainty of CLEO data [27] was taken into account.

A more quantitative test of the CVC hypothesis can be made by comparing the measured  $\tau \rightarrow \omega\pi\nu_\tau$  branching fraction with the value calculated from the  $e^+e^- \rightarrow \omega\pi^0$  cross section according to the formula [3, 27]

$$\Gamma(\tau^- \rightarrow \omega\pi^-\nu_\tau) = \frac{G_F^2 |V_{ud}|^2}{64\pi^4 \alpha^2 m_\tau^3} \int^{m_\tau} q^3 (m_\tau^2 - q^2)^2 (m_\tau^2 + 2q^2) \sigma_{\omega\pi^0}(q) dq, \quad (15)$$

where  $|V_{ud}|$  is the Cabibbo-Kobayashi-Maskawa matrix element,  $m_\tau$  is the  $\tau$  lepton mass,  $G_F$  is the Fermi constant. We integrate the fitted curve shown in Fig. 4 and obtain the value of the product  $\Gamma(\tau^- \rightarrow \omega\pi^-\nu_\tau)B(\omega \rightarrow \pi^0\gamma) = (3.68 \pm 0.04 \pm 0.13) \times 10^{-6}$  eV. Using the values of the  $\tau$  lifetime and  $B(\omega \rightarrow \pi^0\gamma)$  we calculate the branching fraction

$$B(\tau^- \rightarrow \omega\pi^-\nu_\tau) = (1.96 \pm 0.02 \pm 0.10) \times 10^{-2}. \quad (16)$$

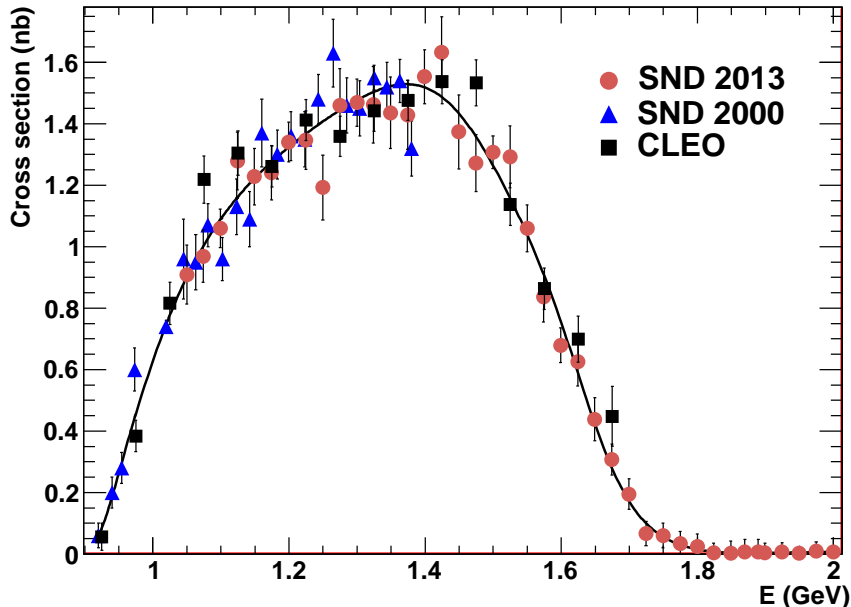


FIG. 6: The cross section for  $e^+e^- \rightarrow \omega\pi^0 \rightarrow \pi^0\pi^0\gamma$  measured in this work (circles) and in Ref. [5] (triangles). Only statistical errors are shown. The cross-section data shown by squares was calculated under CVC hypothesis from the spectral function of the  $\tau \rightarrow \omega\pi\nu_\tau$  decay measured in CLEO experiment [27]. The curve is the result of the fit to SND 2013 and SND 2000 data.

which is in good agreement with the experimental value  $(1.95 \pm 0.08) \cdot 10^{-2}$  obtained as a difference of the PDG [15] values for  $B(\tau^- \rightarrow \omega h^- \nu_\tau)$  and  $B(\tau^- \rightarrow \omega K^- \nu_\tau)$ . We conclude that the CVC hypothesis for the  $\omega\pi$  system works well within the reached experimental accuracy of about 5%.

### VIII. SUMMARY

The cross section for the  $e^+e^- \rightarrow \omega\pi^0 \rightarrow \pi^0\pi^0\gamma$  process has been measured with the SND detector at the VEPP-2000  $e^+e^-$  collider in the energy range of 1.05–2.00 GeV. This is the most accurate measurement of the  $e^+e^- \rightarrow \omega\pi^0$  cross section between 1.4 and 2.0 GeV. Below 1.4 GeV our data agree with the earlier measurements of the same reaction performed at the VEPP-2M collider with the SND [5] and CMD-2 [6] detectors. Significant disagreement is observed with DM2 data [10] in the energy range 1.3–2.0 GeV.

Data on the  $e^+e^- \rightarrow \omega\pi^0$  cross section are well described by the VMD model with the three  $\rho$ -like state:  $\rho(770)$ ,  $\rho'$  and  $\rho''$ . However, the full data set on the  $\gamma^* \rightarrow \omega\pi^0$  transition form factor including data from both  $e^+e^-$  annihilation and  $\omega$  decays, in particular,  $\omega \rightarrow \pi^0\mu^+\mu^-$  [26], cannot be described by such a simple model.

We have also tested the CVC hypothesis comparing the energy dependence of the  $e^+e^- \rightarrow \omega\pi^0$  cross section with the spectral function for the  $\tau^- \rightarrow \omega\pi^- \nu_\tau$  decay, and calculating the branching fraction for this decay from  $e^+e^-$  data. We have concluded that the CVC hypothesis for the  $\omega\pi$  system works well within the experimental accuracy of 5%.

We would like to thank S.Ivashyn for useful discussions. This work is supported by the Ministry of Education and Science of the Russian Federation (Contract 14.518.11.7003), the Russian Federation Presidential Grant for Scientific Schools NSh-5320.2012.2, RFBR (grants 11-02-00276-a, 12-02-00065-a, 13-02-00418-a, 13-02-00375-a 12-02-31488-mol-a, 12-02-31692-mol-a, 12-02-31488-mol-a, 12-02-33140-mol-a-ved), the Russian Federation Presidential Grant for Young Scientists MK-4345.2012.2 and the Grant 14.740.11.1167 from the Federal Program “Scientific and Pedagogical Personnel of Innovational Russia”.

---

[1] Yu. M. Shatunov *et al.*, in Proceedings of the 7th European Particle Accelerator Conference, Vienna, 2000, p.439.

- [2] M. N. Achasov *et al.*, Nucl. Instrum. Meth. A **598**, 31 (2009); V. M. Aulchenko *et al.*, *ibid.* A **598**, 102 (2009); A. Yu. Barnyakov *et al.*, *ibid.* A **598**, 163 (2009); V. M. Aulchenko *et al.*, *ibid.* A **598**, 340 (2009).
- [3] Y.-S. Tsai, Phys. Rev. D **4**, 2821 (1971) [Erratum-*ibid.* D **13**, 771 (1976)].
- [4] S. I. Dolinsky *et al.*, Phys. Lett. B **174**, 453 (1986).
- [5] M. N. Achasov *et al.* (SND Collaboration), Phys. Lett. B **486**, 29 (2000).
- [6] R. R. Akhmetshin *et al.*, (CMD-2 Collaboration), Phys. Lett. B **562**, 173 (2003).
- [7] V. M. Aulchenko *et al.* (SND Collaboration), J. Exp. Theor. Phys. **90**, 927 (2000) [Zh. Eksp. Teor. Fiz. **117**, 1067 (2000)].
- [8] F. Ambrosino *et al.* (KLOE Collaboration), Phys. Lett. B **669**, 223 (2008).
- [9] M. N. Achasov *et al.* (SND Collaboration), JETP Lett. **94**, 2 (2012).
- [10] D. Bisello *et al.*, Nucl. Phys. Proc. Suppl. **21**, 111 (1991).
- [11] M. N. Achasov *et al.* (SND Collaboration), JETP **96**, 789 (2003).
- [12] R. R. Akhmetshin *et al.* (CMD-2 Collaboration) Phys. Lett. B **466**, 392 (1999).
- [13] E. V. Abakumova *et al.*, Phys. Rev. Lett. **110**, 140402 (2013) arXiv:1211.0103 [physics.acc-ph].
- [14] F. A. Berends and R. Kleiss, Nucl. Phys. B **186**, 22 (1981).
- [15] J. Beringer *et al.* (Particle Data Group), Phys. Rev. D **86**, 010001 (2012).
- [16] K. S. Cranmer, Comput. Phys. Commun. **136**, 198 (2001).
- [17] B. Aubert *et al.* (BABAR Collaboration), Phys. Rev. D **76**, 092005 (2007) [Erratum-*ibid.* D **77**, 119902 (2008)].
- [18] B. Aubert *et al.* (BABAR Collaboration), Phys. Rev. D **70**, 072004 (2004).
- [19] E. A. Kuraev and V. S. Fadin, Sov. J. Nucl. Phys. **41**, 466 (1985) [Yad. Fiz. **41**, 733 (1985)].
- [20] G. Bonneau and F. Martin, Nucl. Phys. B **27**, 381 (1971).
- [21] L. G. Landsberg, Phys. Rept. **128**, 301 (1985).
- [22] S. Pacetti, Eur. Phys. J. A **38**, 331 (2008).
- [23] R. R. Akhmetshin *et al.* (CMD-2 Collaboration), Phys. Lett. B **613**, 29 (2005).
- [24] M. N. Achasov *et al.* (SND Collaboration), JETP **107**, 61 (2008).
- [25] R. I. Dzhelyadin *et al.* Phys. Lett. B **102**, 296 (1981) [JETP Lett. **33**, 228 (1981)].
- [26] R. Arnaldi *et al.* (NA60 Collaboration), Phys. Lett. B **677**, 260 (2009).
- [27] K. W. Edwards *et al.* (CLEO Collaboration), Phys. Rev. D **61**, 072003 (2000).